2017-05-25

UPPSALA
UNIVERSITET

Identification of elements and molecules in the spectra of an M dwarf star using high resolution infrared spectroscopy.

Markus Pudas

Examensarbete C i fysik VT 2017, 15.0 hp

Institutionen för fysik och astronomi

Uppsala universitet

Handledare: Ulrike Heiter

Ämnesgranskare: Paul Barklem

Abstract

Context: M dwarfs are abundant and long-lived stellar objects. The formation of planets around stars in stellar systems is believed to be metallicity dependent. To determine the metallicity with synthetic spectrum analysis, the elements producing the absorption lines of the spectra first have to be identified.

Aims: The aim of this thesis is to identify and list the elements or molecules that produce the absorption lines in the spectra of Barnard's star.

Method: This thesis was done at the Division for Astronomy and Space Physics at Uppsala University. High resolution infrared spectral data recorded in the J band 1.1–1.4 μm was downloaded from the CRIRES-POP database. The data had to be wavelength corrected due to the effects of Doppler shift. A modified IDL program was used to read the data files, normalize the flux to unity and plot the spectra. This procedure was also done with the telluric spectra using data from a solar flux atlas. The IDL program plotted the normalized spectra together in the same plot. With this procedure the absorption features originating from the earth’s atmosphere could be identified and discarded. The analysis of the spectral lines resulted in wavelength values which were tested against the VALD3 database to determine what elements were possibly responsible for the absorption features.

Results: The results are presented in a line list. It can be used with other software programs to determine the metallicity. The identified elements and molecules agrees in part with earlier measurements of stellar spectra from M dwarf stars except for a number of lines where no matching elements were found in the VALD3 database.

Conclusions: A line list with possible elements in the photosphere of Barnard’s star can be constructed from the spectra using high-resolution infrared spectroscopy.

Sammanfattning

M dvärgstjärnor är de mest förekommande stjärnorna i vår galax. De har en mycket lång livslängd, vissa tusen gånger längre än vår sol. Det finns teorier om att planetbildning runt stjärnor styrs av halten av ämnen som inte är väte eller helium. Denna halt kallas metallicitet. För att på konstgjord eller syntetisk väg bestämma metalliciteten i Barnard's stjärna, en M dvärg, behöver de ämnen som bidrar till absorptionslinjerna i fotosfären först identifieras. Målsättningen med detta arbete var att identifiera de grundämnen och eventuella molekyler som skapar absorptionslinjerna i spektrumet till Barnard's stjärna.

Detta arbete utfördes på institutionen för fysik och astronomi. Metoden använde ett modifierat IDL program för att läsa och plotta data. Högupplöst infraröd spektraldata från J bandet (1.1–1.4 μm) till Barnard's stjärna hämtades från CRIRES-POP databasen och data för det telluriska spektrumet från en databas med telluriska linjer. Därefter plottades de samtidigt i ett våglängdsöverlappande normaliserat spektra. I programmet gick absorptionslinjer som inte hade sitt ursprung i jordens atmosfär att urskilja manuellt. Då våglängderna för absorptionlinjerna bestämts, matades värden in i databasen VALD3.

Analysen av de returnerade värdena från VALD3 genererade en resultatlista med de mest sannolika elementen för de olika absorptionsvåglängderna. Resultatlistan kan användas som ingångsvärde till program som syntetiskt beräknar metalliciteten. Resultaten överensstämmer till viss del med tidigare mätningar. Slutsatsen är att metoden med högupplöst infraröd spektral data kan användas för att bestämma en lista med element och molekyler från fotosfären i Barnard's stjärna.

Key words. M dwarf stars; line list ; spectroscopy ; high resolution infrared; telluric spectra

Table of Contents

1 Introduction

This chapter gives a short introduction to M dwarf stars and their properties including habitable zones and detection of exoplanets. I also present some data and information of the research object in this work, Barnard's star and reasons for metallicity determination. Some techniques for investigating these stellar objects are also mentioned.

The coolest members of the Morgan Keenan System of stellar spectral classification (MKS) are the M type Red dwarfs. M dwarfs by definition range in effective surface temperature between 2200 K < T_{eff} < 4000 K (Pettersen, 1980). Their masses range from 0.075 to 0.6 solar masses but some literature specifies the range up to 0.8 solar masses (Delfosse et al., 2000). The spectral class definition is of the M or K class and the stars are called dwarfs because they are small compared to the later stages of their evolution. They are main sequence stars according to the Hertzsprung-Russell diagram (HRD) and fuse hydrogen into helium under stable conditions for a very long time period. A red dwarf star remains on the main sequence for a much longer time than our sun since it has lower mass (Laughlin et al., 1997) . The lower masses of red dwarfs reduce the intensity of the fusion process in the core and the reactions rate of hydrogen into helium is slower. Red dwarfs are also more convective which means that they convert a larger amount of the available hydrogen more efficiently. A red dwarf star can remain on the main sequence burning hydrogen into helium up to a thousand times longer than our sun. M dwarfs constitute approximately 70% of the stellar population in our galaxy making them the most abundant stellar object in our neighborhood (Bochansky, 2010; Bastian et al., 2010). It is believed that many of them have orbiting exoplanets which solely by statistics makes them interesting as research objects and specifically in the search for habitable planets.

The habitable zone (HZ) of an M dwarf is much closer than the earth's distance from our sun due to the lower luminosity. The habitable zone is defined as where an atmosphere of CO_2–H_2O–N_2 in gaseous form and H_20 in liquid form can be sustained on the surface of a terrestrial mass planet in a circular region around a star (Kopparapu et al., 2013). This proximity of planets orbiting M dwarfs can increase the possibility of detecting exoplanets within the HZ of the stars.

The radial velocity (RV) method and transit method are common methods of detecting exoplanets in which the former increase in success probability with strong gravitational pull and the latter with

more frequent transits. The transit method is dependent on the exoplanet transiting in front of the line of sight from the observing position. Naturally the number of revolutions increase with closer orbits because a higher velocity is needed to maintain a Keplerian orbit around an object. The fact that red dwarfs are smaller and subsequently less massive leads to larger radial velocity variations, the force or pull of gravity from orbiting planets is proportional to the mass of the objects. Today it is possible to detect a terrestrial mass exoplanet (0.3-10 M_e) with modern techniques (Kopparapu et al., 2013).

Perturbations of the M dwarf star's movement from planets orbiting are thus more easily detected by the RV method. Higher transit frequencies for M dwarf planets are also beneficial when trying to analyze the atmospheres of the exoplanets (Lindgren et al., 2016). Since M dwarfs have been around from the time the Galaxy formed, reasons for research interest are for understanding the chemical evolution of galaxies and evolution of the universe through the initial mass function (IMF) (Scalo, 1986).

Metallicity of stars is defined as the amount of chemical elements in its composition except hydrogen and helium. Metallicity is believed to be linked with a number of interesting models for planetary formation, which all are not yet accurately tested or proven (Buchhave et al., 2014). It is believed that planetary formation is determined by the metallicity in the accretion disc surrounding a newly forming star. For stars of F, G and K type it has been shown that there is a correlation between the stellar metallicity and the occurrence of giant planets (e.g Fischer & Valenti 2005). There have been several metallicity investigations using different techniques on M dwarfs (Bonfils et al., 2005; Chavez and Lambert, 2009; Royas-Ayala et al., 2010; Terrien et al., 2015; Lindgren et al. 2016). Most of these methods are photometric calibrations using different filters but Lindgren et al. (2016) uses high-resolution spectroscopy in combination with binary companions. Metallicity determination is important for several other reasons, including calibration of extragalactic distance measurements using the Cepheid period-luminosity relation (Kudritzki et al., 2013) and how the metallicity of stars affects the evolutionary path.

Barnard's star or V2500 Oph is the fourth closest star to our solar system[1] situated at a distance of 1.82 parsec (pc) (Koen et al., 2010), approximately 5.9 light years. Barnard's Star is red dwarf star of M4 V spectral type with a surface temperature of around 3100K and an apparent visual magnitude of +9.511. The apparent magnitude makes it impossible for the naked eye to see Barnard's star from the earth, the limit is about +6 (Kirkpatrick et al., 1991). Barnard's star is quite

1 http://www.recons.org/TOP100.posted.htm

old, between 7.5 - 11 billion years (Gyr) and it belongs to population II. Population II are older types of stars with lower metallicity compared our sun which is a population I. Barnard's star is also the star with the highest known proper motion, -798 and +10328.12 milliarc seconds per year in right ascension (ra) and declination (dec), respectively and a radial velocity of –110.51 km/s from a heliocentric frame which gives it a redshift z of approx –0.000369 (Nidever, 2002; Van leeuwen et al., 2007).

2 Purpose

The goal of this project is to identify the elements or molecules of a specific star, in this case Barnard's star to create a line list. The resulting line list can be used to produce a synthetic spectral fitting to an observed spectrum in order to determine the metallicity.

I analyzed the highly resolved spectra of Barnard's star, a red dwarf 5.9 light years distant. Because of its vicinity, the red dwarf star makes an important object for detailed studying how metallicity affects red dwarfs attributes and evolution. As stated by Lindgren et al. (2016), accurate abundance analysis is challenging and demands a deep knowledge and understanding of the physics where spectral lines are created. One important tool for investigating the physics of stars is high-resolution spectroscopy. The ability to identify atomic and molecular absorption lines is important in order to find limits of main stellar parameters like metallicity, effective temperature and gravity (Reiners et al., 2007). The first step in metallicity determination using synthetic spectra is to find the elements involved in the creation of the spectral features. These are collected into a line list which is part of the input to other computer programs that analyze and produce a synthetic spectra. Usually the values of the input parameters have to be changed empirically by trial and error to reproduce the best fit between the observed and the synthetically produced spectra.

3 Method

This chapter describes the method for finding the possible elements of the line list from the process of downloading the high-resolution infrared datasets. Further it describes how the motion of earth and the sun affects the measurements, how the IDL (Interactive data language) program in a UNIX environment was used and how the telluric line features were dealt with in the spectra. This chapter also contains a description of how the atomic transitions for the line list were retrieved and the analysis behind it.

3.1 Data

Astronomical spectroscopy can be performed from space-based telescopes or earth-based telescopes using CCD cameras. When spectral measurements are made from earth based telescopes a number of things like the earth's relative motion to the sun and the atmosphere's impact have to be compensated for. These effects are discussed in chapter 3.2 and 3.3 below. In this work I used spectroscopic data from the CRIRES-POP database library (Lebzelter et al., 2012). It is a library containing high-resolution, high signal to noise (S/N) spectra from 1 to 5 µm for stars all across the HRD collected with European Southern Observatory (ESO) telescopes at the La Silla Paranal Observatory in Chile. CRIRES is a high-resolution infrared echelle spectrograph which is a cryogenic cooled CCD instrument attached to the ESO- VLT (Very Large Telescope) at an altitude of 2648 m above sea level. The observations were made on four different occasions in 2010 and 2011. I used CRIRES-POP (Lebzelter et al., 2012) data from the YJ band in this work. The data was partially processed with a pipeline using a standardized method. To achieve better results, further steps are needed, wavelength calibration and correction for telluric lines (Lebzelter et al., 2012).

3.2 Reference frame compensation

The motion of the earth relative to the sun shifts the observed spectrum depending on time of year and if the earth is moving towards or away from the object. The reference values for stars movements in the literature are relative to the the sun. If the relative motion of the earth is towards the object of interest, the stellar spectrum is blue shifted and if the motion is away from the observed object this redshifts the spectra. The information of time and date of each measurement is

stored in the header of the files downloaded from the data section of the CRIRES-POP home page (Lebzelter et al., 2012). The data from the CRIRES-POP database was obtained at several different dates during 2010 and 2011. Barnard's star has a high proper motion and its radial velocity relative to the sun is –110,5 km/s moving towards us, this implies that its spectrum will be blue shifted. Due to the fact that the data files were recorded at different dates the motion of the earth will Doppler shift the spectra in different directions (Lebzelter et al., 2012). The date, place and time of observation from the file header was used to retrieve the true radial velocity on each recording occasion with the ESO Sky Calender Tool[2]. The star's position with coordinates using right ascension and declination from the heliocentric reference frame was used as input. Position and time of the recording on earth including elevation above sea level gave values with which the Doppler shift was calculated for the absorption lines.

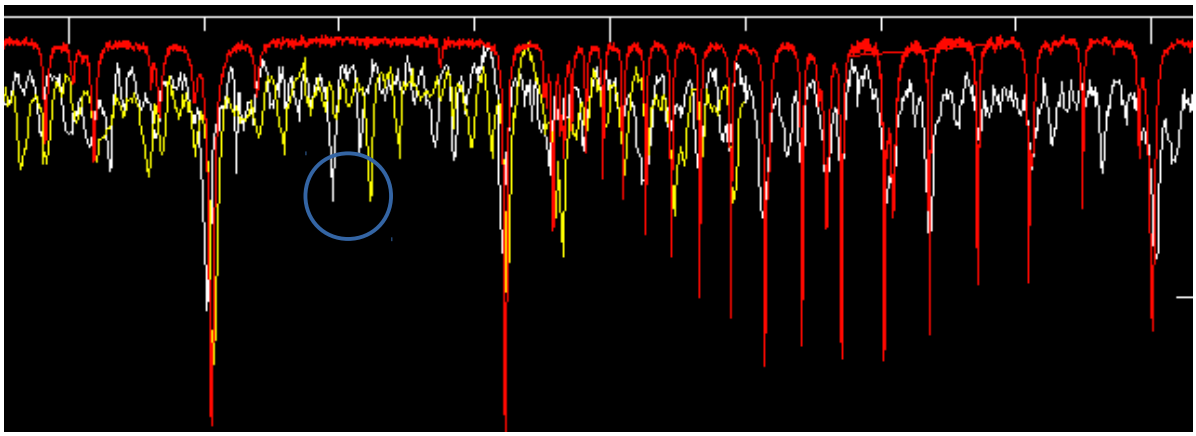

Figure 1: Spectra between 12160 – 12200 Å, with tick marks every 5 Å on x-axis. Y-axis is normalized to unity showing relative strength of absorption lines, tick on the right at 0,2. Showing stellar spectra from two different detectors and dates in white and yellow. The red features is the telluric spectra. Blue circle in figure shows two Doppler shifted absorption lines which are probably the same titanium feature, approximate relative strength of 0,12.

Absorption lines are features in the measured spectra which look like downward pointing spikes. These are created when the continuum emission radiation from the star's surface passes through the surrounding photosphere. Some photons in the continuum radiation have the specific amount of energy that is absorbed by atoms and molecules in the photosphere. This creates the "spikes" in figure 1 and these occur at specific wavelength's since the energy of a photon is connected to its frequency or wavelength.

2 https://www.eso.org/sci/observing/tools/calendar/airmass.html

The white and yellow features in Figure 1 are depicting part of the same wavelength interval but they are offset due to the Doppler effects of the earth's motion. This occurs since the measurements in this case were done on two different dates.

3.3 Telluric lines

The telluric lines are features in the spectrum that originate from the atomic and molecular composition of the earth's atmosphere. These lines contaminate the observed spectra from the astronomical object of interest and it is necessary to remove or minimize their impact as much as possible in order to increase precision and avoid errors.

One of the dominant features in the near IR telluric spectra comes from water vapor (H_2O). The density of H_2O molecules differs due to time of day or season and also by altitude and position on earth. This makes it necessary to have a very good synthetic model or accurate knowledge of the atmospheric composition in the area of measurement at the actual date and time, because the spectra will change on different dates (Lallement et al., 1993). This is referred to as different air masses by astronomers. Other features producing telluric lines are O_2 gaseous oxygen, O_3 Ozone, CO_2 carbon dioxide and CH_4 methane.

There exists several methods for reducing the telluric spectrum (Seifert et al., 2010; Vacca et al., 2003; Lallement et al., 1993; Rudolf et al., 2016). One method which can be used is observation of an A or B class star as a telluric template (Vacca et al., 2003). These stars have generally few metallic features and when observed from the same location just after or before observing the desired object the conditions for the atmospheric composition are equal. This makes the A class star observation a template which can be used to remove the telluric features from the observed spectra. A stars are often fast rotating causing Doppler broadening and if hydrogen lines from the A star are close to the lines of interest in the observed spectra this is not a good method (Vacca et al., 2003). Interstellar dust and gas in the line of observation may also cause Rayleigh scattering of the reference spectra called reddening. One downside with this method is that the strong hydrogen lines from the stars complicates the reduction process but Rudolf et al. (2016) presented a method using IDL programming to reduce this obstacle. The IDL software package tellrem with a line-by-line

radiative transfer model (LBLRTM) results in an increase of errors statistical flux errors in regions affected by telluric lines relative to regions unaffected on the percent level and they conclude that it is an alternative to the telluric template from A or B stars (Rudolf et al., 2016).

In this work I used the atlas of telluric spectrum from (Livingstone & Wallace, 1991) and a modified program based on IDL. The IDL program plots the normalized data from the observed spectra and the normalized data from the telluric lines in the same plot (Figure 2). The telluric lines in figure 2 are easily detected and the strengths are proportional but there is a small shift in wavelength compared with the stellar spectra in white, which could be related to the Doppler shift.

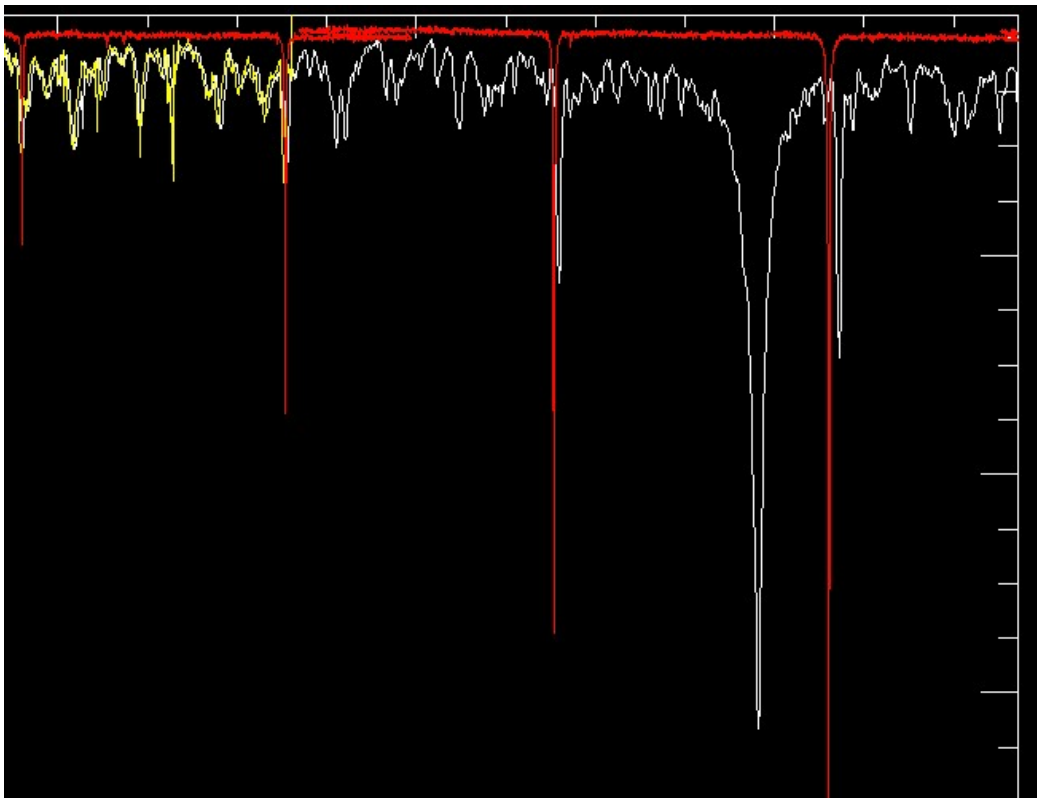

Figure 2: Spectral region between 12475 – 12530 Å with tick marks every 5 Å. Y-axis is normalized to unity showing ticks on the right from 0 to 0,65, relative strength. The telluric lines from the solar atlas in red and the stellar spectra plotted in white (Chip 3). The strong white absorption feature with relative strength of 0,63 is probably a potassium line at 12522.134 Å.

3.4 Programs

The commercial computer language IDL, astro[3] and coyote graphics libraries[4] were used for reading and plotting the data. The astro library contains procedures which can be used and modified when

3 http://idlastro.gsfc.nasa.gov./

4 http://www.idlcoyote.com

needed. In this project I was provided with a IDL program modified by my supervisor to read and plot the fits data files from CRIRES-POP library (Lebzelter et al., 2012) and the ascii tables containing telluric data from Livingstone and Wallace (1991). The datafiles downloaded were in the fits format (Flexible Image Transport System) which is the standard data format used in astronomy applications. It can be used for storing images and spectra but also ascii and binary tables. The files also contain a header that provides information about the data. The fits format is supported by NASA and the International Astronomical union. The provided IDL programme also used a package called astro and a script which merged the CRIRES-POP data files that are segmented in frequency intervals of a few angstrom.

3.5 Linelist

In the ideal world there would be a delta function for the different transitions but in reality there are several mechanisms responsible for the shape of the spectra. The resonance frequency of an atomic transition that one looks for is when the quanta of energy from the photons are interacting with atoms or molecules in the stellar photosphere. In reality this is not an infinitely narrow and accurate resonance frequency described by a delta function. The line shape might also be assumed symmetric but that is not always the case and without understanding the line shape incorrect assumptions could be made. Without understanding the mechanisms that creates broadening of the lines it is difficult to accurately interpret spectroscopic information.

In order to create a line list the frequency position of the transition and the excitation energy and the oscillator strengths are required but additional parameters which govern collisional broadening or Landé factors can be included (Masseron et al., 2014). These data can be found in the on-line VALD3 database (Piskunov et al., 1995; Kupka et al., 1999).

In the process of creating a line list which can be used as input data in a software program like *Spectroscopy Made Easy* (SME) (Valenti & Piskunov, 1996), several things have to be accounted for. First the atoms and molecules in the earth's atmosphere blends the incoming radiation of interest and therefore the measurement which makes the intensity ratios of the radiation important, some features in the spectra might be hidden due to the telluric lines. If the telluric lines are stronger in intensity overcorrection can create false features in the resulting spectra. Detection of the absorption belonging solely to the telluric spectra must be compensated for in order to not draw wrong conclusions about elements in the photosphere of the observed object.

3.6 Analysis

Using absorption lines from the highly resolved infrared or near infrared spectrum from a red dwarf star to extract the metallicity is not an easy task (Lindgren et al., 2016). M dwarfs stars are not that luminous and their cool atmospheres in comparison with other stars can contain a lot of different molecules which makes it more difficult to measure the flux from the star (Schlaufman & Laughlin, 2010). Molecules of TiO and VO in the atmosphere of these stars decrease the bolometric flux due to increased opacity in the visual band (Lindgren et al., 2016). Delfosse et al. (2000) concluded that the magnitude of the infrared spectrum of M stars were not so sensitive to these effects. One important step in improving metallicity determination came in 2005 when Bonfils et al. (2005a) used FGK-dwarfs binaries with M stars. This method is a photometric calibration that relies on the assumption that the stars in the binary system where made from the same primordial gas cloud. This makes it possible to determine the metallicity of individual M dwarfs by calibration against the measured spectra of binaries containing M dwarfs and FGK dwarfs. Determination of red dwarf metallicity with effective temperature below 3500 K has not been widely done with high-resolution spectroscopy.

The analysis of the stellar spectrum can include evaluating strength of the telluric lines and determining what impact they have on the absorption lines. There is more information to be extracted from weak lines but it is difficult to identify which lines to use and which to discard when extracting lines from a plot where telluric and stellar lines are plotted together (Figure 3).

Depending on the resolution level it is difficult to distinguish atomic or molecular lines from the telluric lines. The plot is a normalized superposition of the telluric and stellar spectra. The strength of the downloaded telluric lines depended on the specific conditions the day that they were detected and measured (Livingstone & Wallace, 1991) . The CRIRES data were measured and collected on several different dates which means that and the line formation properties are probably not exactly identical in strength and shape.

Some of the telluric features seen in the Figure 3 below could vary in strength depending on weather conditions at the time of measurement and could be mistaken for noise or produce absorption lines interpreted as coming from the stellar spectra. It is only the stellar features that are Doppler shifted and if a telluric feature is accidentally measured, the Doppler shift compensation of

this line could result in the wrong conclusions about its origin. If this happens it is possible that the resulting synthetic spectra does not match the observed spectra at a later stage of the metallicity determination process. A different method to compensate for the atmospheric effects could then be used.

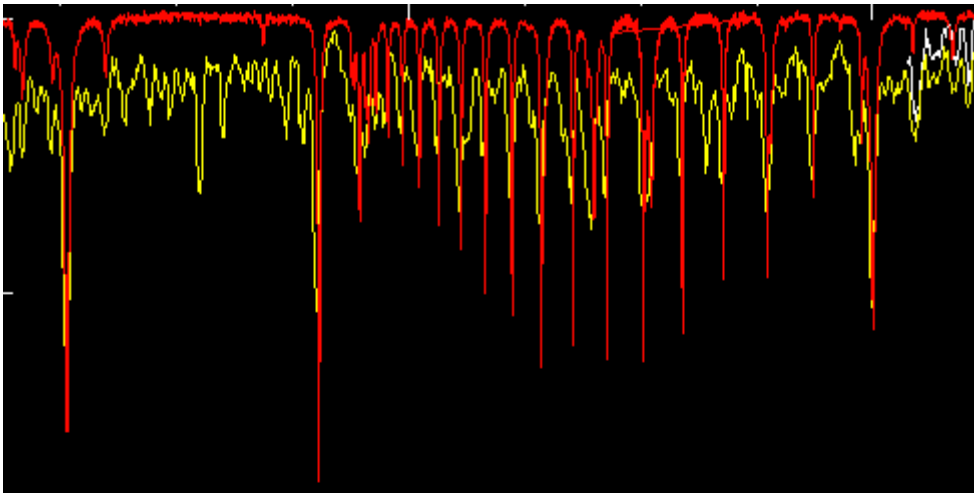

Figure 3: Stellar spectra in yellow, white and Telluric spectra in red, spectral region 12160-12200 Å on x-axis. Y-axis, first tick on left relative strength of 0,2. It is difficult to resolve stellar absorption features from noise and telluric lines.

When analysing a probable absorption feature the wavelength value together with relative strength have to be measured in the IDL plot. Then the extract stellar mode in VALD3 (Piskunov et al., 1995; Kupka et al., 1999) is used over a wavelength interval which covers this specific feature. Extract stellar uses input data like effective temperature, surface gravity, chemical composition, microturbulence and detection threshold. This mode ”*extracts all spectral lines with highest ranked data producing significant absorption for specific stellar atmospheric conditions*” as is stated in the VALD3 homepage. The output is then compared with the measured data and included or discarded depending on fit.

The VALD3 database does not yet include stellar atmosphere models below 3500 K(Piskunov et al., 1995; Kupka et al., 1999). Since Barnard’s effective temperature is between 3100 K < Teff < 3200 K this was compensated for when extracting probable atomic or molecular lines from VALD3

by increasing metallicity by 1 dex relative to solar metallicity. There is a relation between metallicity and opacity which means that an increase in metallicity simulates a lower effective temperature for the stellar atmosphere models in VALD3. The VALD3 database contains data for all chemical elements detected in stellar atmospheres in atomic form, and for a limited number of diatomic molecules (TiO, MgH, CH, SiH, OH, CN)[5].

4 Results

In this chapter I only present parts of the result, the complete line list can be found in the appendix. In table 1 some of the possible elements that could be producing the absorption lines in the spectrum of Barnard's star are shown. Table 2 in the appendix present all measurements including those wavelengths where no matching element was found using this method. A number of identified lines correspond to the lines of the studies by Lindgren et al. (2016) and Lyubchik et al. (2007). These are coloured in table 2 and verifies parts of the results and the identified lines represents a possible start for determining the metallicity.

The resulting lines also meets the goal of this project, to determine a list of elements that can be used for further analysis. Table 1 below gives some of the probable elements for a number of strong and weak lines. Calcium, iron, magnesium, potassium, sodium, and titanium are likely candidates for producing strong lines in the spectra. Titanium, vanadium, silicon and hydroxide are probable for representing the weaker lines of the spectra.

5 Http://www.astro.uu.se/valdwiki/VALD3linelists

Table 1:

Species	*Wavelength [Å]*	*Relative strength*
Na1	11381.441	0.744
Cr	11390.750	0.438
Na1	11403.766	0.740
Fe1	11422.319	0.659
Fe1	11607.572	0.741
K1	11690.220	0.770
K1	11772.838	0.769
Mg1	11828.171	0.578
OH1	11969.915	0.016
Ti1	11973.847	0.492
Mg1	12083.649	0.294
Si1	12103.534	0.018
Fe1	12227.112	0.088
Ti1	12336.954	0.047
OH1	12403.463	0.120
V1	12468.589	0.010
Ti1	12484.617	0.093
OH1	12499.503	0.023
K1	12522.134	0.735
Ca1	12816.045	0.457
Ti1	12831.445	0.486
Mn1	12899.760	0.675
Ca1	13033.554	0.416
Fe1	13206.686	0.082

The absorption feature in figure 2 at 12522.134 Å is seen here in table 1. The high resolution infrared data is collected in 50 Å intervals and the used IDL program only plots these intervals. There would be a possibility to plot the entire spectra in one figure but it would not be useful for extracting any absorption features and the resolution would decrease substantially to fit this document.

5 Discussion

The calculations produced lines that corresponded with Lindgren et al. (2016) and Lyubchik et al. (2007) , this shows that the results are somewhat reliable. A number of lines did not match any extracted line data which could imply that the models need to be changed or modified since the M dwarfs of Lindgren at al. (2016) study all were above 3500K. The line at 12932,524 Å (Table 2) is identified by Lyubchik et al. (2007) as water or iron hydride but the VALD3(Piskunov et al., 1995; Kupka et al., 1999) resulting line of highest probability is a nickel feature (Note that VALD3 does not contain any data for water or FeH).

In the case where no probable matches were found in the returned data from VALD3 (Piskunov et al., 1995; Kupka et al., 1999) further analysis is necessary. When using the extract all function, further lines matching in wavelength, with reasonable excitation energy and oscillator strength further lines appear. These could be candidates to be used in a trial and error process for later metallicity determinations, the difference here that the expected strengths are not calculated. Some of the the lines in table 2 might also be noise instead of real signal as mentioned earlier. The reference library at VALD3 is also not complete and therefore it could be possible to find line data for lines with a match elsewhere.

The uncertainty in how the macroscopic turbulence affects the spectrum has to be considered when determining which absorption lines that connects with line data from elements or molecules. In combination with the measurement and instrument errors, these effects can result in significant uncertainty when determining the centeral wavelength of the absorption feature . In this project the CRIRES-POP data were collected at several different dates of the year. Processes like time dependent convection or variabilities of some kind could affect the stellar spectra differently at different dates. If this is the case it is very difficult to find and determine abundances using data from different occasions.

5.1 Blending

Blending occurs where more than one element or molecule are the cause of absorption. The lines at 13355,443 Å and 11783,145 Å (Table 2) are examples of measurements that have two possible candidates returned from VALD3 (Piskunov et al., 1995; Kupka et al., 1999). The conditions for the telluric features also need to be well known otherwise they will contribute to the uncertainty of the measurements. Possible absorption lines could be blended by telluric lines and this has to be accounted for when determining the metallicity.

5.2 Error estimation

To manually measure an absorption feature using the method described above, a person has to move the mouse pointer across a computer screen and point where the center of the absorption line is believed to be situated. This work has to be done with precision because the mouse pointer resolution is 0.1 Å. The true line centers are also difficult to confirm when they are broad or when the lines are blended.

Another source for uncertainty comes from the determination of the Doppler shift. This effect could be substantial since only a percent difference in determining the radial velocity of Barnard's star gives a relative wavelength shift of approximately $3{,}69*10^{-6}$. This produces a relative wavelength of +/- 498 mÅ at 13500 Å. In this work i have used the value of radial velocity from the paper by Nidever et al. (2002) and they claim systematic errors of 0.4 km/s for M dwarfs which propagates to a change in wavelength of approx +/- 18mÅ at 13500 Å.

5.3 Instrument errors

Measuring the same lines in spectra obtained on different dates results in a wavelength difference which could be originating from instrument deviation. In this work the procedure for measuring a line was performed by one person. The process of measuring was probably done in the same way resulting in similar errors. The line at 11664.2 Å (Table 2) for example was measured on detector 2 in June 2010 and again at March 2011, this time on detector 3. The resulting difference in wavelength was 0.126 Å which points to a instrumental error. There could also be a measurement

error of the relative line strengths if possible spikes from detector are featured in the spectra (Figure 4). This will affect the probability when determining elements using VALD3 (Piskunov et al., 1995; Kupka et al., 1999) extract stellar since the model also returns a prediction for relative strength.

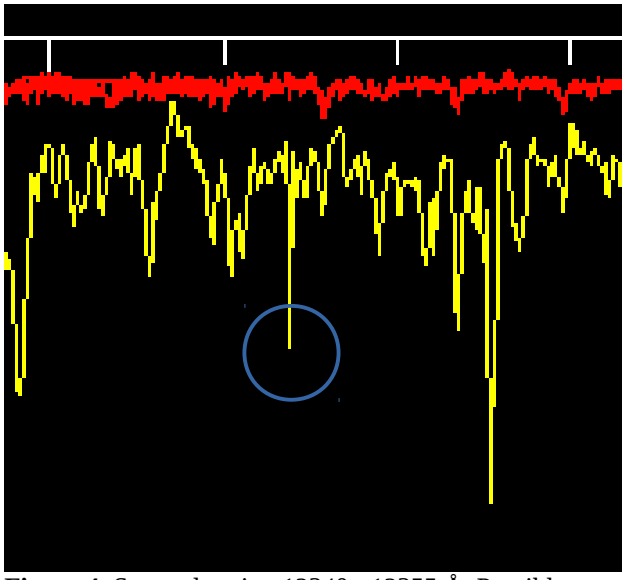

Figure 4: Spectral region 12340 - 12355 Å. Possible spikes from detector creates uncertainty when measuring relative strength. Absorption feature at 12347,539 Å. Blue circle could be 0,07 or 0,03 relative strength

5.4 Resulting error

The resulting combined wavelength errors could reach +/- 0.244 Å when measuring spectral features. This implies an increasing probability that more elements and molecules will match the criteria when determining a line list which could be used as input for synthetic stellar atmosphere calculations. The estimated wavelength error for the measurements is consistent with Luybchik et al. (2007) who infers +/- 0.3 Å error in their study of stars of class M6 to L0 in the J band.

5.5 Future progression

To make progress in this project and determine the metallicity it is possible to use software packages like for instance the Spectroscopic Made Easy, SME (Valenti & Piskunov, 1996) to create a synthetic spectra to fit an observational spectra of Barnard's to determine the metallicity. Installation and running of this program requires some work and a familiarity with UNIX and IDL.

The MARCS models are one type of available model atmosphere calculated by Gustafsson et al. (2008) and they produced a grid of about 10000 model atmospheres for stars within the range of 2500 K≤ T_{eff} ≤ 8000 K. Barnard's star with its surface temperature of 3100K falls in the MARCS model category and an analysis using the software programs of a highly resolved infrared spectrum from CRIRES spectrograph in the J-band (1.1-1.4um wavelength) can be performed. Allard (2012) however concludes that for M dwarfs, the BT-Settl models based on the Asplund et al. (2009) solar abundances produces the most accurate model atmosphere. These model atmospheres are used in the software program to create the synthetic spectrum which is compared to the observed spectrum. The metallicity is then determined by choosing the model parameters such that the synthetic spectrum matches the observed one.

6 Conclusions

It is possible to find elements in the spectra of M dwarfs using high-resolution spectroscopy as was the goal outlined in the purpose section. Elements or possible blends of elements are found for most of the strong lines. Regarding weak lines some elements are distuingishable in the spectra but many of the lines are not found which could be explained by the lack of model atmospheres in VALD3 (Piskunov et al., 1995; Kupka et al., 1999) for this temperature range. A conclusion from this is that the VALD3 database does not include all of the absorption lines found in the stellar atmosphere of Barnard’s star. Some of the identified strong lines have more than one candidate which indicates possible blending.

7 References

Allard, F., Homeier, D., Freytag, B., & Sharp, C. M. (2012). Atmospheres from very low-mass stars to extrasolar planets. *EAS Publications Series*, *57*, 3-43.

Allard, F., Homeier, D., & Freytag, B. (2012). Models of very-low-mass stars, brown dwarfs and exoplanets. *Phil. Trans. R. Soc. A*, *370*(1968), 2765-2777.

Asplund, M., Grevesse, N., Sauval, A. J., & Scott, P. (2009). The chemical composition of the Sun. *Annual Review of Astronomy and Astrophysics*, *47*, 481-522.

Baraffe, I., Chabrier, G., Allard, F., & Hauschildt, P. (2001). Pre-Main Sequence models for low-mass stars and brown dwarfs. In *Symposium-International Astronomical Union* (Vol. 200, pp. 483-491). Cambridge University Press.

Bastian, N., Covey, K. R., & Meyer, M. R. (2010). A universal stellar initial mass function? A critical look at variations. *Annual Review of Astronomy and Astrophysics*, *48*, 339-389.

Bailey, J. M., & Slater, T. F. (2003). A review of astronomy education research. *Astronomy Education Review*, *2*(2), 20-45.

Bochanski, J. J., Hawley, S. L., Covey, K. R., West, A. A., Reid, I. N., Golimowski, D. A., & Ivezić, Ž. (2010). The luminosity and mass functions of low-mass stars in the galactic disk. II. The field. *The Astronomical Journal*, *139*(6), 2679.

Bonfils, X., Delfosse, X., Udry, S., Santos, N. C., Forveille, T., & Ségransan, D. (2005). Metallicity of M dwarfs-I. A photometric calibration and the impact on the mass-luminosity relation at the bottom of the main sequence. *Astronomy & Astrophysics*, *442*(2), 635-642.

Bonfils, X., Forveille, T., Delfosse, X., Udry, S., Mayor, M., Perrier, C., ... & Bertaux, J. L. (2005). The HARPS search for southern extra-solar planets-VI. A Neptune-mass planet around the nearby M dwarf Gl 581. *Astronomy & Astrophysics*, *443*(3), L15-L18.

Buchhave, L. A., Bizzarro, M., Latham, D. W., Sasselov, D., Cochran, W. D., Endl, M., ... & Marcy, G. W. (2014). Three regimes of extrasolar planet radius inferred from host star metallicities. *Nature*, *509*(7502), 593-595.

Chavez, J., & Lambert, D. L. (2009). Isotopic Titanium Abundances in Local M Dwarfs. *The Astrophysical Journal*, *699*(2), 1906.

Delfosse, X., Forveille, T., Ségransan, D., Beuzit, J. L., Udry, S., Perrier, C., & Mayor, M. (2000). Accurate masses of very low mass stars: IV Improved mass-luminosity relations. *arXiv preprint astro-ph/0010586*.

Fischer, D. A., & Valenti, J. (2005). The planet-metallicity correlation. *The Astrophysical Journal*, *622*(2), 1102.

Gizis, J. E. (1996). M-subdwarfs: spectroscopic classification and the metallicity scale. *arXiv preprint astro-ph/9611222*.

Gustafsson, B., Edvardsson, B., Eriksson, K., Jørgensen, U. G., Nordlund, Å., & Plez, B. (2008). A grid of MARCS model atmospheres for late-type stars-I. Methods and general properties. *Astronomy & Astrophysics*, *486*(3), 951-970.

Kirkpatrick, J. D., Henry, T. J., & McCarthy Jr, D. W. (1991). A standard stellar spectral sequence in the red/near-infrared-Classes K5 to M9. *The Astrophysical Journal Supplement Series*, *77*, 417-440.

Koen, C., Kilkenny, D., Van Wyk, F., & Marang, F. (2010). UBV (RI) C JHK observations of Hipparcos-selected nearby stars. *Monthly Notices of the Royal Astronomical Society*, *403*(4), 1949-1968.

Kopparapu, R. K., Ramirez, R., Kasting, J. F., Eymet, V., Robinson, T. D., Mahadevan, S., ... & Deshpande, R. (2013). Habitable zones around main-sequence stars: new estimates. *The Astrophysical Journal*, *765*(2), 131.

Kudritzki, R. P., Urbaneja, M. A., Gazak, Z., Macri, L., Hosek Jr, M. W., Bresolin, F., & Przybilla, N. (2013). A Direct Stellar Metallicity Determination in the Disk of the Maser Galaxy NGC 4258. *The Astrophysical Journal Letters*, *779*(2), L20.

Kupka, F., Piskunov, N. A., Ryabchikova, T. A., Stempels, H. C., & Weiss, W. W. (1999). VALD–2: Progress of the Vienna Atomic Line Data Base. *Astronomy and Astrophysics Supplement Series*, *138*(1), 119-133.

Lallement, R., Bertin, P., Chassefiere, E., & Scott, N. (1993). Correction of spectra for telluric absorption lines with the help of a molecular data bank and high resolution forward modelling: H, O lines around the sodium doublet at 589.5 NM. *Astronomy and Astrophysics*, *271*, 734.

Laughlin, G., Bodenheimer, P., & Adams, F. C. (1997). The end of the main sequence. *The Astrophysical Journal*, *482*(1), 420.

Lebzelter, T., Seifahrt, A., Uttenthaler, S., Ramsay, S., Hartman, H., Nieva, M. F., ... & Hussain, G. A. J. (2012). CRIRES-POP-A library of high resolution spectra in the near-infrared. *Astronomy & Astrophysics*, *539*, A109.

Lépine, S., Hilton, E. J., Mann, A. W., Wilde, M., Rojas-Ayala, B., Cruz, K. L., & Gaidos, E. (2013). A spectroscopic catalog of the brightest (J< 9) M dwarfs in the northern sky. *The Astronomical Journal*, *145*(4), 102.

Lindgren, S., Heiter, U., & Seifahrt, A. (2016). Metallicity determination of M dwarfs-High-resolution infrared spectroscopy. *Astronomy & Astrophysics*, *586*, A100.

Livingston, W., & Wallace, L. (1991). An atlas of the solar spectrum in the infrared from 1850 to 9000 cm-1 (1.1 to 5.4 micrometer). *NSO Technical Report, Tucson: National Solar Observatory, National Optical Astronomy Observatory, 1991*.

Lyubchik, Y., Jones, H. R., Pavlenko, Y. V., Martin, E., McLean, I. S., Prato, L., ... & Tennyson, J. (2007). Spectral analysis of high resolution near-infrared spectra of ultra cool dwarfs. *Astronomy & Astrophysics*, *473*(1), 257-264.

Mann, A. W., Brewer, J. M., Gaidos, E., Lépine, S., & Hilton, E. J. (2013). Full metal bracket: A calibration of infrared and optical spectroscopic metallicities of M dwarfs over 1.5 dex. *Astronomische Nachrichten*, *334*(1-2), 18-21.

Mann, A. W., Feiden, G. A., Gaidos, E., Boyajian, T., & von Braun, K. (2015). How to constrain your M dwarf: measuring effective temperature, bolometric luminosity, mass, and radius. *The Astrophysical Journal*, *804*(1), 64.

Masseron, T., Plez, B., Van Eck, S., Colin, R., Daoutidis, I., Godefroid, M., ... & Christlieb, N. (2014). CH in stellar atmospheres: an extensive linelist. *Astronomy & astrophysics*, *571*, A47.

Nidever, D. L., Marcy, G. W., Butler, R. P., Fischer, D. A., & Vogt, S. S. (2002). Radial velocities for 889 late-type stars. *The Astrophysical Journal Supplement Series*, *141*(2), 503.

Önehag, A., Heiter, U., Gustafsson, B., Piskunov, N., Plez, B., & Reiners, A. (2012). M-dwarf metallicities. A high-resolution spectroscopic study in the near infrared. *Astronomy & Astrophysics*, *542*, A33.

Pepe, F., Mayor, M., Galland, F., Naef, D., Queloz, D., Santos, N. C., ... & Burnet, M. (2002). The CORALIE survey for southern extra-solar planets VII-Two short-period Saturnian companions to HD 108147 and HD 168746. *Astronomy & Astrophysics*, *388*(2), 632-638.

Piskunov, N. E., Kupka, F., Ryabchikova, T. A., Weiss, W. W., & Jeffery, C. S. (1995). VALD: The Vienna Atomic Line Data Base. *Astronomy and Astrophysics Supplement Series*, *112*, 525.

Pettersen, B. R. (1980). Physical parameters of solar neighbourhood flare stars. *Astronomy and Astrophysics*, *82*, 53-60.

Rajpurohit, A. S., Reylé, C., Allard, F., Scholz, R. D., Homeier, D., Schultheis, M., & Bayo, A. (2014). High-resolution spectroscopic atlas of M subdwarfs. Effective temperature and metallicity. *Astronomy & Astrophysics*, *564*, A90.

Reiners, A., Homeier, D., Hauschildt, P. H., & Allard, F. (2007). A high resolution spectral atlas of brown dwarfs. *Astronomy & Astrophysics*, *473*(1), 245-255.

Rojas-Ayala, B., Covey, K. R., Muirhead, P. S., & Lloyd, J. P. (2012). Metallicity and temperature indicators in M dwarf K-band spectra: Testing new and updated calibrations with observations of 133 solar neighborhood M dwarfs. *The Astrophysical Journal*, *748*(2), 93.

Rudolf, N., Günther, H. M., Schneider, P. C., & Schmitt, J. H. M. M. (2016). Modelling telluric line spectra in the optical and infrared with an application to VLT/X-Shooter spectra. *Astronomy & Astrophysics*, *585*, A113.

Scalo, J. M. (1986). The stellar initial mass function. *Fundamentals of cosmic physics*, *11*, 1-278.

Schlaufman, K. C., & Laughlin, G. (2010). A physically-motivated photometric calibration of M dwarf metallicity. *Astronomy & Astrophysics*, *519*, A105.

Seifahrt, A., Käufl, H. U., Zängl, G., Bean, J. L., Richter, M. J., & Siebenmorgen, R. (2010). Synthesising, using, and correcting for telluric features in high-resolution astronomical spectra-A near-infrared case study using CRIRES. *Astronomy & Astrophysics*, *524*, A11.

Soubiran, C., Bienaymé, O., Mishenina, T. V., & Kovtyukh, V. V. (2008). Vertical distribution of Galactic disk stars-IV. AMR and AVR from clump giants. *Astronomy & Astrophysics*, *480*(1), 91-101.

Terrien, R. C., Mahadevan, S., Deshpande, R., & Bender, C. F. (2015). A Near-Infrared Spectroscopic Survey of 886 Nearby M Dwarfs. *The Astrophysical Journal Supplement Series*, *220*(1), 16.

Van Leeuwen, F. (2007). Validation of the new Hipparcos reduction. *Astronomy & Astrophysics*, *474*(2), 653-664.

Valenti, J. A., & Piskunov, N. (1996). Spectroscopy made easy: A new tool for fitting observations with synthetic spectra. *Astronomy and Astrophysics Supplement Series*, *118*(3), 595-603.

Woolf, V. M., & Wallerstein, G. (2006). Calibrating M dwarf metallicities using molecular indices. *Publications of the Astronomical Society of the Pacific*, *118*(840), 218.

Vacca, W. D., Cushing, M. C., & Rayner, J. T. (2003). A Method of Correcting Near-Infrared Spectra for Telluric AbsorptionBased on observations obtained with the Infrared Telescope Facility, which is operated by the University of Hawaii under contract to the National Aeronautics and Space Administration. *Publications of the Astronomical Society of the Pacific*, *115*(805), 389.

https://www.eso.org/sci/observing/tools/calendar/airmass.html

http://www.univie.ac.at/crirespop/data.htm

https://fits.gsfc.nasa.gov/

https://idlastro.gsfc.nasa.gov/ftp/

http://vald.astro.uu.se/~vald/php/vald.php

ftp://vso.nso.edu/pub/Wallace_telluric_near_ir_atlas/README.pdf

9 Acknowledgements

- *I would like to acknowledge my supervisor Ulrike Heiter, for all the help, support and discussions doing this thesis.*
- *NSO/Kitt Peak FTS data used here were produced by NSF/NOAO.*
- *This work has made use of the VALD database, operated at Uppsala University, the Institute of Astronomy RAS in Moscow, and the University of Vienna.*

10 Appendix

The data in table 2 presents the measured absorption features found in the J band and the resulting probable line-transitions chosen from the VALD3 output using the extract stellar mode. The first column is the measured and Doppler shift compensated value in angstrom (Å). Second column is the measured relative strength where 1 is maximum value. Third column is the returned short format from VALD3 when increasing metallicity with 1 dex in the extract stellar mode. Other input data in VALD3 extract stellar mode were T_{eff} 3500 K, microturbulence 1 km/s, detection threshold 0.01, surface gravity 4.5 in cgs units. Third column is in order specie or ion, wavelength in vacuum for the transition in angstrom (Å), excitation potential in electron volt (eV), microturbulence in km/s, log statistical weight times oscillator strength, log Radiative damping constant, log Quadratic Stark damping constant at l0000 K, van der Waals damping parameter, landé factor, central depth and last referens. Where ”No data in VALD3” appears this means that no probable matching line data was returned from the extract stellar mode.

Coloured rows in table 2 corresponds to lines also found in two papers using high resolution spectroscopy on M dwarfs. Luybchik et al. (2007) on a M6 dwarf among other stars and Lindgren et al. (2016) on M dwarfs hotter than 3500 K.

Same line as Lindgren et al.(2016)

Same as Lyubchik et al. (2007)

Same as Lindgren and Lyubchik

Table 2

Wavelength (Å)	relative strength	VALD3 Result
11373,992	0,22	OH 1', 11373.984, 1.2819, 1.0, -6.388, 0.000, 0.000, 0.000,99.000, 0.011, ' 1 GSGCD
11381,295	0,75	Na 1', 11381.441, 2.1023, 1.0, -0.466, 0.000, 0.000,-7.109,99.000, 0.744, ' 7 NIST10
11385,197	0,26	Ca 1', 11385.259, 4.7435, 1.0, -2.039, 7.920,-3.090,-6.860, 1.500, 0.017, ' 4 K07
		OH 1', 11385.234, 1.5790, 1.0, -5.620, 0.000, 0.000, 0.000,99.000, 0.020, ' 1 GSGCD
11388,305	0,53	Fe 1', 11388.538, 5.6207, 1.0, -0.711, 8.510,-4.970,-7.500, 1.600, 0.014, ' 2 K14
11390,704	0,21	Cr 1', 11390.750, 3.3223, 1.0, -0.423, 7.860,-5.760,-7.640, 1.670, 0.438, ' 5 WLHK
11391,704	0,26	No data in VALD3.
11403,71	0,82	Na 1', 11403.766, 2.1044, 1.0, -0.165, 0.000, 0.000,-7.109,99.000, 0.740, ' 7 NIST10
11422,418	0,41	Fe 1', 11422.319, 2.1979, 1.0, -2.700, 7.150,-6.220,-7.820, 1.980, 0.659, ' 2 K14
11422,217	0,48	No data in VALD3.
11432,819	0,33	No data in VALD3
11436,625	0,19	OH 1', 11436.758, 1.2659, 1.0, -6.111, 0.000, 0.000, 0.000,99.000, 0.022, ' 1 GSGCD
11479,538	0,21	No data in VALD3.
11484,539	0,18	Cr 1', 11484.630, 3.3223, 1.0, -0.226, 7.860,-5.760,-7.640, 1.170, 0.478, ' 1 WLHK
11517,249	0,13	OH 1', 11517.138, 1.7429, 1.0, -5.621, 0.000, 0.000, 0.000,99.000, 0.012, ' 7 GSGCD
11532,155	0,27	No data in VALD3
11554,180	0,29	No data in VALD3.
11554,780	0,12	No data in VALD3.
11590,196	0,09	No data in VALD3.
11583,293	0,07	No data in VALD3.
11596,799	0,15	No data in VALD3.
11600,901	0,12	No data in VALD3.
11607,503	0,5	Fe 1', 11607.572, 2.1979, 1.0, -2.009, 7.160,-6.220,-7.820, 1.660, 0.741, ' 1 K14
11620,208	0,17	No data in VALD3.
11626,113	0,2	No data in VALD3.
11633,515	0,13	No data in VALD3.
11632,793	0,37	No data in VALD3.
11633,293	0,39	No data in VALD3.
11634,915	0,15	No data in VALD3.
11638,695	0,51	Fe 1', 11638.260, 2.1759, 1.0, -2.214, 7.170,-6.220,-7.820, 1.580, 0.721, ' 1 K14
11639,695	0,59	No data in VALD3.
11642,220	0,12	No data in VALD3.
11642,696	0,23	No data in VALD3.
11644,721	0,09	No data in VALD3.
11645,097	0,17	No data in VALD3.
11646,422	0,12	No data in VALD3.
11646,798	0,18	No data in VALD3.
11647,698	0,12	OH 1', 11647.304, 1.3052, 1.0, -5.814, 0.000, 0.000, 0.000,99.000, 0.037, ' 7 GSGCD
11648,198	0,13	OH 1', 11647.812, 1.3053, 1.0, -5.814, 0.000, 0.000, 0.000,99.000, 0.037, ' 7 GSGCD
11654,601	0,19	No data in VALD3.
11655,601	0,16	Al 1', 11655.222, 4.8272, 1.0, -0.999, 0.000, 0.000, 0.000,99.000, 0.030, ' 1 K75
11656,101	0,14	No data in VALD3.
11656,501	0,16	No data in VALD3.
11661,729	0,15	No data in VALD3.
11662,296	0,11	No data in VALD3.
11664,330	0,12	No data in VALD3.
11664,204	0,13	No data in VALD3.
11664,302	0,23	No data in VALD3.
11664,502	0,23	No data in VALD3.

Wavelength (Å)	relative strength	VALD3 Result
11665,003	0,29	No data in VALD3.
11674,106	0,12	No data in VALD3.
11675,506	0,14	OH 1', 11675.948, 1.1905, 1.0, -5.542, 0.000, 0.000, 0.000,99.000, 0.093, ' 4 GSGCD
11682,837	0,13	No data in VALD3.
11682,811	0,16	No data in VALD3.
11690,140	0,72	K 1', 11690.220, 1.6100, 1.0, 0.250, 7.810,-5.170,-7.326,99.000, 0.770, ' 8 WSM
		Fe 1', 11689.972, 2.2227, 1.0, -2.068, 7.150,-6.220,-7.820, 2.000, 0.727, ' 5 K14
11691,612	0,14	No data in VALD3.
11692,112	0,14	No data in VALD3.
11696,814	0,09	No data in VALD3.
11697,914	0,07	No data in VALD3.
11700,815	0,12	No data in VALD3.
11701,117	0,13	No data in VALD3.
11715,821	0,13	No data in VALD3.
11717,421	0,08	No data in VALD3.
11728,826	0,08	OH 1', 11728.342, 1.1090, 1.0, -6.226, 0.000, 0.000, 0.000,99.000, 0.031, ' 3 GSGCD
11728,827	0,13	No data in VALD3.
11729,321	0,11	No data in VALD3
11734,323	0,11	No data in VALD3.
11747,034	0,15	No data in VALD3.
11749,234	0,07	No data in VALD3.
11751,136	0,15	No data in VALD3.
11751,835	0,09	No data in VALD3.
11753,636	0,11	No data in VALD3.
11759,538	0,17	No data in VALD3.
11769,642		No data in VALD3.
11772,741	0,57	K 1', 11772.838, 1.6171, 1.0, 0.510, 7.810,-5.170,-7.326,99.000, 0.769, ' 3 WSM
11780,446	0,13	Ti 1', 11780.542, 1.4432, 1.0, -2.170, 6.870,-6.100,-7.790, 1.210, 0.339, ' 5 LGWSC
11783,145	0,19	Fe 1', 11783.265, 2.8316, 1.0, -1.574, 6.750,-6.150,-7.820, 1.140, 0.633, ' 8 K14
		Mn 1', 11783.433, 5.1334, 1.0, -0.094, 8.400,-5.200,-7.560, 1.350, 0.012, ' 10 K07
11785,946		OH 1', 11786.021, 1.2438, 1.0, -5.497, 0.000, 0.000, 0.000,99.000, 0.086, ' 1 GSGCD
11795,049	0,11	Ca 1', 11795.763, 4.5347, 1.0, -1.008, 7.500,-3.530,-7.090, 1.330, 0.179, ' 2 K07
11824,903	0,16	No data in VALD3.
11825,804	0,15	No data in VALD3.
11828,105	0,18	Mg 1', 11828.171, 4.3458, 1.0, -0.333, 0.000, 0.000,-7.192,99.000, 0.578, ' 3 NIST10
11831,606	0,49	No data in VALD3.
11836,008	0,13	No data in VALD3.
11836,809	0,15	No data in VALD3.
11837,609	0,18	No data in VALD3.
11842,411	0,15	No data in VALD3.
11889,633	0,14	OH 1', 11889.565, 1.2038, 1.0, -6.198, 0.000, 0.000, 0.000,99.000, 0.024, ' 4 GSGCD
11890,433	0,08	Fe 1', 11890.487, 5.5392, 1.0, -0.544, 8.200,-4.300,-7.450, 1.160, 0.028, ' 2 K14
11891,133	0,09	Ca 1', 11891.119, 4.6813, 1.0, -2.237, 7.910,-3.200,-6.990, 1.210, 0.015, ' 1 K07
11892,834	0,12	Ti 1', 11892.877, 1.4298, 1.0, -1.730, 6.930,-6.100,-7.790, 0.750, 0.440, ' 5 LGWSC
11898,537	0,08	No data in VALD3.
11899,737	0,08	No data in VALD3.
11903,239	0,1	OH 1', 11903.172, 1.3008, 1.0, -5.456, 0.000, 0.000, 0.000,99.000, 0.078, ' 4 GSGCD
11906,240	0,1	OH 1', 11906.178, 1.3018, 1.0, -5.455, 0.000, 0.000, 0.000,99.000, 0.078, ' 4 GSGCD
11914,244	0,1	No data in VALD3.

Wavelength (Å)	relative strength	VALD3 Result
11916,745	0,1	OH 1', 11916.708, 1.2516, 1.0, -5.684, 0.000, 0.000, 0.000,99.000, 0.058, ' 4 GSGCD
11933,552	0,13	No data in VALD3.
11938,454	0,17	No data in VALD3.
11939,654	0,1	No data in VALD3.
11940,255	0,1	No data in VALD3.
11941,455	0,12	No data in VALD3.
11943,356	0,09	No data in VALD3.
11944,657	0,09	No data in VALD3.
11949,359	0,13	OH 1', 11949.157, 1.4119, 1.0, -5.451, 0.000, 0.000, 0.000,99.000, 0.055, ' 1 GSGCD
		Ga 1', 11949.230, 3.0734, 1.0, 0.000, 0.000, 0.000, 0.000,99.000, 0.079, ' 2 GUES
11949,959	0,35	Ti 1', 11949.547, 1.4432, 1.0, -1.570, 6.900,-6.100,-7.790, 1.000, 0.466, ' 3 LGWSC
11952,160	0,11	No data in VALD3.
11970,168	0,11	OH 1', 11970.172, 1.7137, 1.0, -5.597, 0.000, 0.000, 0.000,99.000, 0.014,
11969,912	0,07	OH 1', 11969.915, 1.7562, 1.0, -5.458, 0.000, 0.000, 0.000,99.000, 0.016,
11971,213	0,09	OH 1', 11971.157, 1.7630, 1.0, -5.502, 0.000, 0.000, 0.000,99.000, 0.015, ' 1 GSGCD
11973,013	0,16	Fe 1', 11973.046, 2.1759, 1.0, -1.483, 7.190,-6.220,-7.820, 1.260, 0.722, ' 7 K14
11973,814	0,59	Ti 1', 11973.847, 1.4601, 1.0, -1.390, 6.870,-6.100,-7.790, 1.140, 0.492, ' 3 LGWSC
11975,014	0,38	No data in VALD3.
11975,714	0,1	No data in VALD3.
11979,716	0,1	OH 1', 11979.956, 1.6950, 1.0, -5.666, 0.000, 0.000, 0.000,99.000, 0.013, ' 1 GSGCD
11980,616	0,11	OH 1', 11980.130, 1.6950, 1.0, -5.666, 0.000, 0.000, 0.000,99.000, 0.013,
11981,316	0,11	OH 1', 11981.451, 1.7870, 1.0, -5.429, 0.000, 0.000, 0.000,99.000, 0.016, ' 1 GSGCD
11982,017	0,11	OH 1', 11981.969, 1.7933, 1.0, -5.469, 0.000, 0.000, 0.000,99.000, 0.014, ' 1 GSGCD
11983,017	0,08	No data in VALD3.
11994,521	0,11	No data in VALD3.
11994,921	0,11	No data in VALD3.
11995,922	0,11	No data in VALD3.
11996,522	0,09	No data in VALD3.
11997,622	0,1	No data in VALD3.
11998,723	0,1	No data in VALD3.
12000,623	0,2	Cr 1', 12000.970, 3.4348, 1.0, -2.068, 6.270,-6.090,-7.790, 1.000, 0.063, ' 4 WLHK
12003,224	0,13	No data in VALD3.
12003,825	0,18	No data in VALD3.
12007,226	0,07	No data in VALD3.
12009,827	0,17	No data in VALD3.
12012,628	0,06	No data in VALD3.
12013,828	0,12	No data in VALD3.
12015,829	0,12	Ti 1', 12015.938, 3.3232, 1.0, -1.016, 7.880,-5.980,-7.750, 0.660, 0.028, ' 7 K10
12016,229	0,13	No data in VALD3.
12025,632	0,16	No data in VALD3.
12026,433	0,12	No data in VALD3.
12029,834	0,1	No data in VALD3.
12032,822	0,11	No data in VALD3.
12058,231	0,07	No data in VALD3.
12063,933	0,06	No data in VALD3.
12069,535	0,08	No data in VALD3.
12078,239	0,09	No data in VALD3.
12081,240	0,08	No data in VALD3.
12083,439	0,23	Mg 1', 12083.649, 5.7532, 1.0, 0.410, 7.470, 0.000,-6.981,99.000, 0.294, ' 6 NIST10
		Mg 1', 12083.346, 5.7532, 1.0, -0.790, 0.000, 0.000, 0.000,99.000, 0.096, ' 5 KP

Wavelength (Å)	relative strength	VALD3 Result
12087,042	0,18	No data in VALD3.
12088,743	0,15	No data in VALD3.
12090,043	0,09	No data in VALD3.
12095,244	0,08	No data in VALD3.
12103,647	0,09	Si 1', 12103.534, 4.9296, 1.0, -0.350, 8.550,-5.220,-7.299, 1.000, 0.018, ' 1 K07
12105,448	0,11	Ca 1', 12105.841, 4.5541, 1.0, -0.305, 7.420,-3.870,-7.090, 1.000, 0.322, ' 3 K07
12106,248	0,1	No data in VALD3.
12108,749	0,14	No data in VALD3.
12119,353	0,15	Fe 1', 12119.494, 4.5931, 1.0, -1.635, 7.340,-6.230,-7.830, 1.120, 0.060, '
12127,956	0,14	No data in VALD3.
12130,658	0,19	No data in VALD3.
12143,363	0,09	No data in VALD3.
12143,863	0,09	No data in VALD3.
12152,466	0,09	No data in VALD3.
12174,375	0,12	Ti 1', 12174.166, 2.1603, 1.0, -3.071, 5.820,-6.010,-7.800, 1.000, 0.017, ' 1 K10
12174,517	0,12	No data in VALD3.
12175,417	0,09	No data in VALD3.
12202,784	0,1	No data in VALD3.
12227,131	0,15	Fe 1', 12227.112, 4.6070, 1.0, -1.368, 8.430,-5.410,-7.540, 1.670, 0.088, ' 3 K14
12231,933	0,06	No data in VALD3.
12248,037	0,07	No data in VALD3.
12255,439	0,08	Ti 1', 12255.699, 3.9215, 1.0, 0.161, 8.280,-5.550,-7.520, 1.070, 0.045, ' 4 K10
12258,040	0,09	No data in VALD3.
12285,041	0,06	No data in VALD3.
12286,442	0,06	No data in VALD3.
12287,842	0,08	Ca 1', 12287.939, 4.8775, 1.0, -1.939, 7.990,-2.790,-6.750, 1.170, 0.015, ' 2 K07
12291,843	0,06	No data in VALD3.
12933,438	0,1	No data in VALD3.
12294,144	0,08	No data in VALD3.
12295,744	0,17	OH 1', 12295.311, 1.4972, 1.0, -5.368, 0.000, 0.000, 0.000,99.000, 0.051, ' 1 GSGCD
12297,945	0,12	No data in VALD3.
12308,725	0,11	No data in VALD3.
12312,926	0,08	No data in VALD3.
12315,627	0,08	No data in VALD3.
12318,128	0,06	No data in VALD3.
12318,929	0,1	No data in VALD3.
12323,931	0,08	No data in VALD3.
12325,931	0,07	No data in VALD3.
12330,533	0,1	No data in VALD3.
12332,834	0,08	No data in VALD3.
12333,434	0,08	No data in VALD3.
12337,135	0,08	Ti 1', 12336.954, 2.1747, 1.0, -2.572, 8.000,-6.010,-7.740, 1.340, 0.047, ' 1 K10
12338,636	0,07	No data in VALD3.
12339,536	0,09	No data in VALD3.
12343,138	0,11	Fe 1', 12342.916, 4.6382, 1.0, -1.463, 8.420,-5.380,-7.540, 2.010, 0.072, ' 2 K14
12343,838	0,12	No data in VALD3.
12347,539	0,07	OH 1', 12347.951, 1.6851, 1.0, -5.562, 0.000, 0.000, 0.000,99.000, 0.017, ' 3 GSGCD
12351,541	0,11	No data in VALD3.

Wavelength (Å)	relative strength	VALD3 Result
12357,343	0,17	No data in VALD3.
12363,144	0,08	No data in VALD3.
12363,844	0,07	No data in VALD3.
12370,847	0,08	No data in VALD3.
12372,548	0,08	No data in VALD3.
12373,648	0,09	No data in VALD3.
12374,248	0,07	No data in VALD3.
12378,150	0,08	No data in VALD3.
12395,356	0,15	No data in VALD3.
12396,757	0,09	No data in VALD3.
12399,158	0,13	No data in VALD3.
12403,460	0,12	OH 1', 12403.463, 2.1865, 1.0, -8.864, 0.000, 0.000, 0.000,99.000, 0.000, ' 10 GSGCD
12405,661	0,11	No data in VALD3.
12407,062	0,1	No data in VALD3.
12410,963	0,11	No data in VALD3.
12412,564	0,11	No data in VALD3.
12415,965	0,13	No data in VALD3.
12416,965	0,12	No data in VALD3.
12419,867	0,1	OH 1', 12419.570, 1.7050, 1.0, -5.445, 0.000, 0.000, 0.000,99.000, 0.021, ' 3 GSGCD
12420,867	0,11	No data in VALD3.
12423,268	0,1	Mg 1', 12423.029, 5.9320, 1.0, -1.188, 0.000, 0.000, 0.000,99.000, 0.034, ' 1 NIST10
12426,769	0,11	No data in VALD3.
12431,971	0,56	K 1', 12432.273, 1.6100, 1.0, -0.439, 7.790,-4.880,-7.022,99.000, 0.715, ' 5 WSM
12435,985	0,09	No data in VALD3.
12438,086	0,09	No data in VALD3.
12440,886	0,06	No data in VALD3.
12442,787	0,06	No data in VALD3.
12443,887	0,08	Ca 1', 12433.748, 5.0261, 1.0, -0.066, 7.940,-3.480,-7.090, 1.000, 0.213, ' 4 K07
12447,088	0,08	No data in VALD3.
12451,089	0,07	No data in VALD3.
12454,190	0,08	No data in VALD3.
12458,791	0,07	No data in VALD3.
12459,592	0,18	No data in VALD3.
12468,794	0,06	V 1', 12468.589, 2.8954, 1.0, -1.460, 6.920,-6.020,-7.780, 1.230, 0.010, ' 3 K09
12473,896	0,06	No data in VALD3.
12477,897	0,09	No data in VALD3.
12484,398	0,1	Ti 1', 12484.617, 1.5025, 1.0, -3.277, 6.870,-6.110,-7.780, 0.440, 0.093, ' 4 K10
12488,099	0,11	No data in VALD3.
12490,000	0,13	No data in VALD3.
12492,500	0,08	No data in VALD3.
12499,002	0,1	No data in VALD3.
12499,602	0,09	OH 1', 12499.503, 1.7288, 1.0, -5.350, 0.000, 0.000, 0.000,99.000, 0.023, ' 2 GSGCD
12501,803	0,06	No data in VALD3.
12502,403	0,06	No data in VALD3.
12504,704	0,04	No data in VALD3.
12506,004	0,08	No data in VALD3.
12522,609	0,63	K 1', 12522.134, 1.6171, 1.0, -0.139, 7.790,-4.880,-7.021,99.000, 0.735, ' 6 WSM
12531,111	0,09	No data in VALD3.
12631,945	0,11	No data in VALD3.

Wavelength (Å) relative strength VALD3 Result

Wavelength (Å)	relative strength	VALD3 Result
12632,445	0,14	No data in VALD3.
12638,147	0,14	Fe 1', 12638.703, 4.5585, 1.0, -0.783, 8.440,-5.410,-7.540, 1.260, 0.210, ' 1 K14
12642,849	0,12	No data in VALD3.
12646,650	0,11	No data in VALD3.
12650,952	0,13	Cr 1', 12651.030, 3.8446, 1.0, -1.724, 6.480,-6.150,-7.780, 1.330, 0.038,
12665,957	0,15	No data in VALD3.
12668,458	0,12	No data in VALD3.
12671,259	0,21	Ti 1', 12671.096, 1.4298, 1.0, -2.360, 6.820,-6.100,-7.790, 1.470, 0.312, ' 5 LGWSC
12671,960	0,21	Cr 1', 12671.340, 3.4379, 1.0, -3.011, 8.260,-5.750,-7.630, 2.760, 0.010, ' 3 WLHK
12680,663	0,34	No data in VALD3.
12738,284	0,21	Ti 1', 12738.383, 2.1747, 1.0, -1.280, 7.950,-6.010,-7.750, 1.020, 0.270, ' 1 LGWSC 1
12776,480	0,06	No data in VALD3.
12790,284	0,07	No data in VALD3.
12801,587	0,07	No data in VALD3.
12806,088	0,06	No data in VALD3.
12811,490	0,14	Ti 1', 12811.478, 2.1603, 1.0, -1.390, 7.990,-6.010,-7.750, 0.950, 0.254, ' 3 LGWSC
12812,290	0,08	No data in VALD3.
12815,991	0,17	Ca 1', 12816.045, 3.9104, 1.0, -0.765, 8.280,-5.220,-7.520, 1.250, 0.457, ' 1 K07
12821,692	0,4	No data in VALD3.
12826,994	0,05	No data in VALD3.
12828,194	0,06	No data in VALD3.
12831,295	0,37	Ti 1', 12831.445, 1.4298, 1.0, -1.490, 6.820,-6.100,-7.790, 0.670, 0.486, ' 3 LGWSC
12836,596	0,06	No data in VALD3.
12837,397	0,06	No data in VALD3.
12844,199	0,05	No data in VALD3.
12847,199	0,38	Ti 1', 12847.034, 1.4432, 1.0, -1.330, 6.820,-6.100,-7.790, 1.080, 0.510, ' 1 LGWSC 1
12849,400	0,05	No data in VALD3.
12853,501	0,06	No data in VALD3.
12854,801	0,07	No data in VALD3.
12856,202	0,05	No data in VALD3.
12857,302	0,05	No data in VALD3.
12858,202	0,07	No data in VALD3.
12880,039	0,14	OH 1', 12880.126, 1.8656, 1.0, -5.120, 0.000, 0.000, 0.000,99.000, 0.027, ' 6 GSGCD
12900,047	0,4	Mn 1', 12899.760, 2.1142, 1.0, -1.070, 0.000, 0.000, 0.000, 1.290, 0.675, ' 1 B-WPNP
12906,749	0,07	No data in VALD3.
12909,350	0,12	Ca 1', 12909.070, 4.4300, 1.0, -0.224, 7.770,-5.830,-7.710, 0.710, 0.390, ' 6 K07
12910,450	0,1	Cr 1', 12910.090, 2.7079, 1.0, -1.779, 7.260,-6.140,-7.800, 1.360, 0.394, ' 7 WLHK
12932,524	0,08	Ni 1', 12932.313, 2.7403, 1.0, -2.523, 7.680,-6.170,-7.810, 0.530, 0.220, ' 11 K08
12937,125	0,09	Cr 1', 12937.020, 2.7099, 1.0, -1.896, 7.260,-6.140,-7.800, 1.500, 0.368, ' 7 WLHK
12953,767	0,07	No data in VALD3.
12966,371	0,07	No data in VALD3.
12988,680	0,06	No data in VALD3.
12990,581	0,07	No data in VALD3.
13011,846	0,16	Ti 1', 13011.897, 1.4432, 1.0, -2.270, 6.820,-6.100,-7.790, 1.490, 0.333, ' 1 LGWSC
13033,395	0,18	Ca 1', 13033.554, 4.4410, 1.0, -0.064, 7.770,-5.830,-7.710, 1.080, 0.416, ' 7 K07
13057,859	0,07	OH 1', 13057.428, 1.8708, 1.0, -5.029, 0.000, 0.000, 0.000,99.000, 0.034, ' 4 GSGCD
		Ga 1', 13057.789, 4.1107, 1.0, 0.500, 0.000, 0.000, 0.000,99.000, 0.011, ' 11 GUES
13076,863	0,21	No data in VALD3.
13150,983	0,51	No data in VALD3.

Wavelength (Å)	relative strength	VALD3 Result
13191,195	0,1	No data in VALD3.
13191,297	0,19	No data in VALD3.
13197,199	0,15	Cr 1', 13197.410, 3.5505, 1.0, -2.647, 6.310,-6.020,-7.790, 1.130, 0.019, ' 6 WLHK
13198,299	0,15	Ti 1', 13198.866, 2.2393, 1.0, -2.841, 5.820,-6.050,-7.800, 1.480, 0.030, ' 8 K10
13206,701	0,13	Fe 1', 13206.686, 0.0516, 1.0, -8.960,-1.490,-6.280,-7.820, 1.500, 0.082, ' 1 K14
13212,603	0,18	Ni 1', 13212.418, 2.7403, 1.0, -3.901, 7.440,-6.190,-7.810, 0.660, 0.024, ' 2 K08
13218,105	0,13	No data in VALD3.
13218,605	0,12	No data in VALD3.
13219,205	0,12	Ti 1', 13219.200, 2.1747, 1.0, -2.614, 6.650,-6.010,-7.810, 0.750, 0.055, ' 6 K10
13219,605	0,11	No data in VALD3.
13227,107	0,15	No data in VALD3.
13234,909	0,11	Rb 1', 13235.170, 1.5596, 1.0, -0.478, 0.000, 0.000, 0.000,99.000, 0.177, ' 7 Wc
13235,610	0,1	No data in VALD3.
13245,912	0,13	No data in VALD3.
13250,111	0,16	Ca 1', 13250.322, 4.5541, 1.0, -1.033, 7.560,-3.980,-7.100, 1.010, 0.199, ' 9 K07
13250,911	0,23	No data in VALD3.
13257,615	0,07	No data in VALD3.
13267,218	0,25	No data in VALD3.
13278,587	0,16	No data in VALD3.
13322,934	0,3	No data in VALD3.
13326,435	0,15	No data in VALD3.
13329,136	0,17	No data in VALD3.
13342,439	0,32	No data in VALD3.
13343,839	0,29	No data in VALD3.
13344,840	0,43	No data in VALD3.
13345,740	0,37	No data in VALD3.
13352,142	0,32	Fe 1', 13352.173, 5.3085, 1.0, -0.521, 8.220,-4.760,-7.490, 1.630, 0.078, ' 4 K14
13355,443	0,35	Cr 1', 13355.444, 6.6587, -6.767, 8.540,-4.940,-7.530, 0.000,' 7 K10 Blending??
		Fe 1', 13355.464, 6.3981, -3.506, 8.270,-4.300,-7.260, 1.220,' 5 K14
13356,043	0,34	Co 1', 13356.067, 5.5242, -1.861, 8.670,-4.580,-7.510, 0.400,' 12 K08
13357,243	0,41	Ti 1', 13357.313, 4.6640, -3.267, 8.340,-5.230,-7.540, 0.590,' 1 K10
		Co 1', 13357.373, 5.9395, -2.785, 8.350,-4.450,-7.440, 0.860,' 12 K08
13362,345	0,39	Co 1', 13362.224, 5.7597, -3.206, 8.290,-5.020,-7.520, 1.900,' 4 K08
13363,445	0,36	V 1', 13363.578, 5.2367, -3.902, 7.850,-3.630,-7.280, 2.690,' 17 K09
		Fe 1', 13363.483, 6.3482, -4.133, 8.260,-4.380,-7.400, 1.600,' 12 K14
13367,246	0,33	Cr 1', 13367.135, 6.6587, -3.727, 8.330,-4.700,-7.340, 1.470,' 4 K10
		Fe 1', 13367.420, 6.3515, -3.312, 8.240,-4.150,-7.330, 1.350,' 6 K14
13368,346	0,34	Ti 1', 13368.290, 4.6089, -2.627, 8.160,-5.130,-7.660, 1.400,' 7 K10
13387,327	0,37	OH 1', 13387.310, 3.4397, -5.734, 0.000, 0.000, 0.000,99.000,' 4 GSGCD
13389,928	0,5	Fe 1', 13389.846, 3.0176, 1.0, -4.620, 6.120,-6.110,-7.810, 0.920, 0.033, ' 1 K14
		Fe 1', 13389.414, 5.3852, 1.0, -0.516, 8.230,-4.720,-7.480, 1.190, 0.066, ' 1 K14
13390,729	0,47	OH 1', 13390.673, 2.0126, 1.0, -4.983, 0.000, 0.000, 0.000,99.000, 0.026, ' 2 GSGCD
13391,329	0,38	No data in VALD3.
13397,031	0,44	K 1', 13397.062, 2.6702, 1.0, -1.660, 7.460,-4.110, 0.000,99.000, 0.101, ' 4 WSM
		OH 1', 13397.296, 2.1198, 1.0, -5.108, 0.000, 0.000, 0.000,99.000, 0.013, ' 2 GSGCD 2
13397,931	0,41	OH 1', 13397.858, 2.1198, 1.0, -5.108, 0.000, 0.000, 0.000,99.000, 0.013, ' 2 GSGCD 2
13401,433	0,5	OH 1', 13401.702, 2.0107, 1.0, -4.961, 0.000, 0.000, 0.000,99.000, 0.027, ' 2 GSGCD
13411,036	0,46	OH 1', 13411.039, 2.0527, 1.0, -4.918, 0.000, 0.000, 0.000,99.000, 0.026, ' 2 GSGCD
13425,642	0,35	No data in VALD3.
13426,042	0,36	No data in VALD3.
13427,342	0,33	No data in VALD3.
13429,643	0,62	No data in VALD3.
13434,945	0,57	No data in VALD3. 'CN 1', 13434.820, 1.6590, -2.698, 6.170, 0.000, 0.000, 99.000 (extract all VALD3)
13435,746	0,48	No data in VALD3.
13437,746	0,33	No data in VALD3.
13438,247	0,22	No data in VALD3. 'Ni 1', 13438.235, 6.0859, -1.401, 8.800,-4.410,-7.310, 1.670,' (Extract all VALD3)